DOI: 10.1002/ ((please add manuscript number))
Article type: Full Paper

Fingertip Skin-Inspired Highly Sensitive and Multifunctional Sensor with Hierarchically Structured Conductive Graphite/Polydimethylsiloxane Foams

Qi-Jun Sun, Xin-Hua Zhao, Ye Zhou, Chi-Chung Yeung, Wei Wu, Shishir Venkatesh, Zong-Xiang Xu, Jonathan J. Wylie, Wen-Jung Li, and Vellaisamy A. L. Roy**

Dr. Q.-J. Sun, Dr. W. Wu, Dr. S. Venkatesh, Dr. V. A. L. Roy
State Key Laboratory of Terahertz and Millimeter Waves and Department of Materials Science & Engineering
Hong Kong SAR 999077, P. R. China
City University of Hong Kong
E-mail: val.roy@cityu.edu.hk

Dr. X.-H. Zhao, Dr. Z.-X. Xu
Department of Chemistry
South University of Science and Technology of China
Shenzhen 518055, P. R. China

Mr. C.-C. Yeung
Department of Chemistry
City University of Hong Kong
Hong Kong SAR 999077, P. R. China

Dr. Y. Zhou
Institute for Advanced Study
Shenzhen University
Shenzhen 518060, P. R. China

Prof. J. J. Wylie
Department of Mathematics,
City University of Hong Kong
Hong Kong SAR 999077, P. R. China

Prof. W.-J. Li
Department of Mechanical Engineering
City University of Hong Kong
Hong Kong SAR 999077, P. R. China

Keywords: skin sensor, microstructure, multifunctional sensing, healthcare monitoring, temperature sensing

Recently, skin sensors have obtained considerable attentions for potential applications in skin prosthetics, healthcare monitoring, and humanoid robotics. In order to further extend the practical applications, a dynamic broad range response with excellent sensitivity is important for skin sensors in sensing pressure, which eventually simplify the sensing system devoid of extra signal processing. On the other aspect, skin sensors with multifunctional sensing

functionalities are highly desirable to satisfy various application requirements. Although diversities of designed microstructures and functional materials have been adopted, achieving skin sensor devices possessing high pressure sensitivity over wide range and multifunctional sensing capabilities are still challenging. Herein, inspired by the microstructures of fingertip skin, we demonstrate skin sensors possessing excellent sensitivity over a wide pressure range and multifunctional sensing capabilities by the structural design of the sensing layer, with surface hierarchical microstructures and inside porous structures. The fabricated skin sensor device exhibits a superior sensitivity of 245 kPa^{-1} over a wide pressure range from 5 Pa to 120 kPa. For practical application demonstrations, the sensor devices are utilized to monitor subtle wrist pulse and diverse human motions including finger bending, wrist bending, and feet movement. Furthermore, this novel sensor device demonstrates potential applications in recognizing textures and detecting environmental temperatures, which make an important progress for constructing advanced electronic skin.

1. Introduction

In the past decade, flexible and stretchable skin sensors have attracted significant interest for their potential applications in skin prosthetics,[1-10] wearable health monitoring systems,[11-24] and humanoid robotics.[25-28] Real-time monitoring physiological signals such as wrist pulse, body temperature, and body motion can provide plentiful valuable information for disease diagnosis and treatment.[11, 13, 15] As the potential applications of skin sensors, tremendous works are being carried out in the development of high-performance skin sensors, including pressure sensors, temperature sensors, and humidity sensors etc.[2-6] Particularly, skin-like pressure sensors, converting the external force into electrical signal, have attracted tremendous attention and the piezoresistive prototype has been intensively explored due to the advantages of simple fabrication procedures and oversimplified signal acquisition. On one hand, pressure sensors possessing high pressure sensitivity and wide linearity range are highly required in health monitoring and artificial intelligence. For examples, a high sensitivity in

subtle pressure range is desirable for wrist pulse monitoring and a high sensitivity in large pressure range is necessary for robotic operations. On the other hand, multifunctional skin sensor devices are highly desirable for e-skin application, which is required to sense the external pressure, texture roughness, and temperature simultaneously. Despite the great efforts in the development of such kind of multifunctional skin sensors, the complicated fabrication procedures and the sophisticated device structures have hindered their practical applications.

With the advances in materials science and engineering, smart and functional materials with nano/microstructures have been extensively used in fabrication of varieties of sensor devices including pressure sensors,[29] strain sensors,[30] and gas sensors.[31] In particular, carbon-based functional materials in the forms of nanotubes,[5, 20] graphene,[2, 22] and graphene oxide[3] have been broadly explored as conductive fillers or sensing elements in skin sensors as a result of their outstanding features of light weight, low cost, high conductivity, and excellent mechanical stability. Furthermore, a variety of microstructures, such as micro-pillars, hemispheres, and triangular pyramid have been introduced in fabrication of skin sensors to improve the performance of the skin sensors such as response time, detection limit, sensing range, and sensitivity.[12, 32-35] As an example, Cheng and co-workers demonstrated a pressure sensor with mimosa-inspired microstructures, achieving a high sensitivity up to 50.17 kPa^{-1} in the low pressure range of 0-70 Pa. However, the sensing range is below 1500 Pa and the sensitivity decreases to 1.38 kPa^{-1} beyond 70 Pa, which confines the sensor to tiny pressure detection.[36] Therefore, its applications in health monitoring and intelligent robotics are limited. In another work reported by Zhang et al.,[37] the pressure sensor device has a wide pressure sensing range of 0-100 kPa based on fingerprint-like graphene as the active layer and a high sensitivity of up to 110 kPa^{-1} is realized in the subtle pressure range of 0-200 Pa. Nevertheless, the sensitivity sharply decreases to 3 kPa^{-1} for the moderate pressure region (0.2-15 kPa) and 0.26 kPa^{-1} for the large pressure region (15-75 kPa), respectively. Thus, great challenges remain in the development of skin sensors by structural design to obtain a high

sensitivity over broad pressure range. Additionally, skin sensors with multifunctional sensing capabilities are intriguing for e-skin applications. Recently, obvious efforts have been paid in developing multifunctional skin sensors based on microstructures. For example, by employing the microstructured ferroelectric film, Ko and co-workers presented a flexible multifunctional skin sensor which can detect the pressure, temperature, and vibration at the same time. Meanwhile, their skin sensors have been demonstrated in detecting wrist pulses and the effects of temperature to the wrist pulses.[6] However, the pressure sensor shows a high sensitivity only in the subtle pressure region. Therefore, despite the impressive achievements, skin sensors possessing high sensitivity over wide linear pressure range and multifunctional sensing abilities for diverse stimuli, are still highly desirable to extend their practical applications.

Varieties of functional materials and microstructures from nature have motivated researchers' inspirations in material engineering, especially the hierarchical microstructures for bioinspired artificial e-skin.[38-41] As the largest organ of human body, skin acts significant roles in mediating human interactions with the surrounding environments. Particularly, the fingertip skin, considered much more sensitive in sensing external stimuli than the other parts of human skin, can sense pressure and temperature due to the special rige structures between the epidermal and dermal layers, transmitting the stimuli from the environment to the sensory receptors located in interlocked rige structures. Moreover, the microstructures on human fingertip skin allow the fingertip a high sensitivity in distinguishing the texture roughness by the friction signals between the fingertip skin and object. Actually, the randomly distributed microstructures both underlying and on the surface of fingertip skin play important roles in external stimulus perception. As far as we know, the fingertip skin inspired highly sensitive skin sensors for sensing multiple external stimuli are quite deficient.

Herein, motivated by the epidermal microstructures from human fingertip skin, we report a novel skin sensor based on conductive Graphite/polydimethylsiloxane (G/PDMS) foam films

with hierarchical microstructures on the surface to detect external stimuli, including pressure, texture roughness, and temperature signals. It is notable that the randomly distributed microstructures on surface of sandpaper have a high similarity in topography with those of human fingertip skin. By using sandpaper as the template to mimic the spinosum microstructures on the fingertip skin and micro graphite sheets as the conductive fillers, skin sensors with high sensitivity and wide sensing range both in pressure and temperature have been achieved. Additionally, cubic sodium chloride (NaCl) templates are employed to obtain the foam structures inside the G/PDMS film to further improve the sensitivity in sensing pressures. Moreover, mimicking the stratum corneum of human fingertip skin, outside microstructures on the substrate of the skin sensor are prepared using the sandpaper template to recognize texture roughness. Based on the novel design of our skin sensor, its applications for the detection of physiological signals (wrist pulse, finger bending, and wrist bending etc.), texture roughness of papers, and environmental temperatures have been successfully demonstrated.

2. Results and discussion

2.1. Fabrication of the skin sensors

Figure 1 depicts the schematic illustrations for the fabrication procedure of the skin sensors. Firstly, the as prepared G/PDMS/NaCl composite ink was coated on the sandpaper template by blading method, followed by covering another piece of sandpaper on the top. Secondly, composite film with double-sided microstructures was obtained after thermal treatment and removal of sandpaper templates. Dipping the composite film into hot water under an ultrasonic bath for 2 hours, NaCl sacrificial templates were removed and the G/PDMS composite film with both porous structures and surficial microstructures (denoted as porous@microstructured) was obtained. Meanwhile, the composite film with only porous structures (denoted as porous@planar) and composite film with only surficial microstructures

(denoted as microstructured only) were prepared for the reference devices. The fabrication procedures for these two films are similar with that of porous@microstructured composite film by using different template combinations, and more detailed fabrication procedures are illustrated in the experimental part. Thirdly, PDMS prepolymer was coated on the sandpaper template followed by covering an indium tin oxide (ITO) coated polyethylene terephthalate (PET) substrate on top with PET-side facing the PDMS to fabricate the outside microstructures on the substrate. After solidified at 100 ^{o}C for 1 h, due to the better attachment between PDMS and PET than that of PDMS and sandpaper, the sandpaper template was easily peeled off and microstructures were formed on the PDMS film. Finally, a sandwiched structure was used to construct the skin sensors by incorporating the porously microstructured composite film between ITO/PET and ITO/PET/PDMS flexible substrates. The scanning electron microscopy (SEM) images of sandpaper template (#120), G/PDMS composite film, and NaCl sacrificial templates are depicted in **Figure 2**. As seen from Figure 2a and 2b, surface heights of the sandpaper template are randomly distributed and hierarchical structures are found on the template. Figure 2d and 2e show the SEM images of G/PDMS composite film with different magnifications. The surface morphology of the composite film shows the randomly distributed ridges and hierarchically microstructured holes derived from the hierarchical structures of the sandpaper. The diameters of the large and small holes are found to be around 150 and 10 μm, respectively, and the sizes are constant with those of the microhumps from the sandpaper. To obtain a low initial conductivity to minimize the power consumption at standby state, and realize an enhanced sensitivity and flexibility of the skin sensor, NaCl sacrificial templates were employed to obtain the porosity inner the composite film. Figure 1f and 1g show the SEM images of NaCl particles and cross-sectional porous sensing layer, respectively. It is notable that the diameters of porous structures inside the sensing layer are similar with the template particles, indicating an effective approach to realize sensing layers with rich porous structures. Meanwhile, surficial microstructured

composite films without porous structures and planar composite films with porous structures were prepared for the reference devices. The SEM image for micro-patterned PDMS layer is depicted in Figure S2 (Supporting Information), showing a similar surface morphology with that of the composite film, which proves that the sandpaper is an effective template in preparing microstructures both on PDMS and G/PDMS composite films.

2.2. Performance of the skin sensor in sensing pressure

As mentioned above, by using different template combinations, three types of composite films were prepared for skin sensors. The as prepared composite films were cut into 1×1 cm^2 in size and sandwiched between top ITO/PET substrate and bottom ITO/PET/PDMS substrate, and copper wires were affixed onto the ITO face as electrodes for external electrical connections. In order to characterize the current responses of the skin sensors to external pressures, a measurement system containing a motorized test stand connected with a force gage, and a semiconductor parameter analyzer was used (Inset of **Figure 3**a). The pressures loaded on the skin sensors were preciously controlled by the force gauge, and the current signals were collected by the analyzer. To evaluate the pressure sensitivity, the relative current variation of the composite film based skin sensors measured under a wide range of external pressures is shown in Figure 3a. Notably, all skin sensors exhibit two linear segments but differential slopes in the same pressure region for these three kinds of skin sensors. The pressure sensitivity (S) can be defined as $S= (\Delta I/I_{off})/\Delta P$, generally utilized to assess the performance of the skin sensors, where I and P are the current of the skin sensors and the applied external pressure, respectively. For the skin sensor with the porous@planar G/PDMS composite film, the estimated pressure sensitivity is 0.04 and 0.02 kPa^{-1} in the pressure range of 0-100 kPa and 100-150 kPa, respectively. The relative low sensitivity is because of the high initial conductivity due to the complete connection between the surfaces of the composite film and the ITO electrodes. As seen from Figure 3a, compared to that of the

porous@planar skin sensor, the device based on the sandpaper-templated without porous microstructures exhibit an improved pressure sensitivity, 46 kPa^{-1} in the pressure range of 0-120 kPa and 21 kPa^{-1} in the pressure range of 120-150 kPa, indicating the surficial microstructures of the composite film acts a significant role in boosting up pressure sensitivity of the skin sensor. It is notable that, among these three types of skin sensors, the device based on porous@microstructured composite film shows the highest sensitivities, and the calculated sensitivities are 245 kPa^{-1} and 90 kPa^{-1}, corresponding to the ranges of 0-120 kPa and 120-150 kPa, respectively. As verified above, the surficial microstructures on the composite film are critical to obtain a high sensitivity. Additionally, compared with the device based on the composite film with only surficial microstructures, the porous structures can further decrease the initial conductivity of the composite film, which is beneficial to the improvement of pressure sensitivity. The detailed discussion for the sensing mechanism will be presented later. Overall, all the three types of skin sensors with G/PDMS composite films exhibit a wide pressure sensing range of up to 150 kPa with varied sensitivities. The performance of our skin sensor compared to the reported state-of-the-art pressure sensors has been listed in Table S1 (Supporting Information). As far as we know, especially for the pressure sensors based on the porous@microstructured composite film, it is scarcely reported devices with such high sensitivities in such wide linearity range. We suppose that a high sensitivity and a wide linearity range are both crucial for the potential extensive applications in sensing subtle and large pressures. Unless otherwise stated, the skin sensors are all based on the porous@microstructured composite film.

To investigate the minimum detectable pressure of the skin sensors, as depicted in Figure 3b, the current responses to pressure were measured by loading/unloading a small grain of red bean (~50 mg, inset of Figure 3b). Notably, the skin sensor exhibits a quick response to the subtle pressure variations (~5 Pa) generated by the loading and unloading of the red bean, and the minimum detectable pressure is comparable to those of the previously reported state-of-

the-art skin sensors.[10, 38-39] For example, reported by Shu and co-workers, a high-performance skin sensor with gold nanowires coated tissue paper as the active layer shows a minimum detectable pressure of 13 Pa.[14] Another work reported a skin sensor based on PVDF@rGO nanofibers exhibits a limit of detection of 1.2 Pa.[3] Furthermore, to investigate the response speed, the response and relaxation time of the skin sensor were estimated in the process of loading/unloading the small grain of red bean, as depicted in Figure 3c. As shown in Figure 3c, it is observed a response and relaxation time of 8 ms and 4 ms, respectively, which even show better performance than those of human skin (~40 ms), indicating its fast pressure response and potential application in e-skin. The greatly reduced hysteresis of the response and relaxation time could be ascribed to the reduced viscoelastic effects of the composite film compared with those of the pure PDMS film. The effects of loading frequency should be considered for evaluating the performance of skin sensors. As depicted in Figure 3d to 3f, frequency-dependent performance of the skin sensor under an applied force of 10 N (~100 kPa) with three different loading frequencies (0.12, 0.20, and 1.10 Hz) has been further investigated. Notably, the current responsive signals closely follow the loaded force, and no obvious frequency dependence or delay is observed within the studied frequency range, demonstrating the skin sensor based on the porous@microstructured G/PDMS is sensitive and stable at different frequencies. To fully reveal the piezoresistive behavior of the skin sensor, its current responses to different pressures under loading/unloading cycles were investigated systematically. The cyclic current responses of the skin sensor to five different pressures are shown in Figure 3g. It is notable that the patterns of every responsive cycle under different pressures are highly identical, demonstrating the skin sensor has an excellent current responsiveness to the applied cyclic pressures, and the current altitudes of the skin sensor rise significantly with the increased external pressures. Interestingly, as shown in Figure 3g, the skin sensor is turned off (the current almost drops to zero) when no external pressure is applied, indicating that our presented skin sensor is a kind of energy-saving device with

almost zero power consumption at standby state, which is different from other reported skin sensors based on the conductive composite film or nanowire networks.[12, 14] Moreover, as shown in Figure 3h, the skin sensor exhibits a robust durability in the process of loading/unloading a huge pressure of 100 kPa up to 25 000 cycles. As we can see in the insets of magnified view, there is no obvious degradation in current amplitude during the whole process of 25 000 loading/unloading test cycles. The excellent durability is attributed to the intrinsic stability of the graphite sheets and strong attachment between the graphite sheets and the PDMS in the composite film.

Due to its excellent performance, our skin sensor possesses the abilities to detect varieties of forces including press force, bending force, and twist force. Additionally, versatile potential applications for detection of subtle physiological signals and human body motion activities have been demonstrated. As shown in **Figure 4**a, once the skin sensor is pressed by human finger, the contact area between the ITO electrodes and the microstructured composite film will increase, and the pores inside the composite film will be simultaneously compressed to induce more conductive pathways, leading to the increase of current correspondingly. After removal of press force, the skin sensor was turned off immediately, further demonstrating that our skin sensor possesses fast response speed and low-power consumption at standby state. In addition to sensing the press force, the skin sensor has been demonstrated in detection of bending force and twist force as shown in Figure 4b and 4c, respectively. To prove their potential applications in humanoid robotics, the skin sensors were attached on five fingertips of a rubber glove (Figure 4d) to monitor the holding and grasping the objects by robotics. Our skin sensors could preciously detect the motion of every finger, and distinguished electrical signals of each gesture (spreading five fingers, holding an aurilave, raising thumbs-up, and holding a beaker) were measured to assess the hand gestures (Figure 4e). In addition, the skin sensors were either attached on the outside of the index finger or human wrist to detect the bending states of index finger and wrist, respectively. As shown in Figure 4f to 4h, once the

index finger or wrist was bent, the conducting area between the electrode and composite film was enlarged, and the current increased correspondingly. The current altitudes of the skin sensor were also found to increase with the enlargement of bending angles. Additionally, in order to imitate the sense of touch of human, as shown in **Figure 5**a, two skin sensors were affixed to a robotic arm to detect the pressures applied on the objects in the process of grasping and release. As depicted in Figure 5b and 5c, we notice that different current altitudes are obtained when grasping objects with different weights, which means different grasping feeling of the robot in the grasping processes of different objects. These results further prove the potential applications of our skin sensor in industrial robotics.

As other application demonstrations, the skin sensor was affixed onto human heel to monitor human feet motions. As depicted in Figures S3a and S3b (Supporting Information), the skin sensor exhibits distinct signal intensities and shapes for walking and running, respectively. A wave signal response with a flat peak was obtained for the normal walking state, and a walking stride frequency of 90/min, while the stride frequency increased to 180/min, and sharp peaks of enhanced signal intensities were observed for the running state. Wrist pulse waveform, one of the important physiological signals, can reveal the health condition of the cardiovascular system. To prove the health monitoring ability, our skin sensor was attached onto the artery of human wrist using the medical tape to detect the pulse in real-time, as shown in Figure S4a (Supporting Information). Owing to the high sensitivity and fast pressure response speed, high resolution wrist pulse waveforms were collected by our skin sensor. Figure S4b (Supporting Information) shows the collected pulse of the volunteer under normal condition, exhibiting a calculated beat frequency of 79 bpm, which is in the healthy category of adults. As shown in Figure S4c (Supporting Information), which is the enlarged view of a wrist pulse picked from Figure S4b, three characteristic peaks named percussion waves, tidal waves, and diastolic wave are observed clearly, indicating its promising potential in disease diagnosis and real-time monitoring of human health.

2.3. Recognition of texture roughness.

Notably, the human fingertip skin has the ability in distinguishing the texture roughness of the objects. Due to the microstructures on the outer side of the flexible substrate, mimicking the microstructures from fingertip skin, our skin sensor is able to detect the slight friction force generated by the sliding of the skin sensor on the test objects to recognize the texture roughness. The schematic diagrams of the device and sensing mechanism are illustrated in **Figure 6**a to 6c. As depicted in Figure 6b, very few connections between the microhumps and ITO electrodes at the standby state. Figure 6c shows that the friction force from the sliding process increased the conductive pathways, and the resistance of the device decreased simultaneously. To confirm this effectiveness, printing paper and sandpapers with different roughness (#800, #120) are chosen for the test. The SEM images of the printing paper, #800 sandpaper, and #120 sandpaper are depicted in Figure 6d-f. In the experiment, the skin sensor was affixed onto the index finger, and the finger was brought to the surface of the papers and moved from one side to the other. In this process, a gentle press force was applied on the sensor and the whole touch-move action takes 10 seconds from start to end. As shown in Figure 6g-i, due to the different friction forces generated in the sliding process with three different roughness, distinct patterns were obtained when the skin sensor slides across these three different surfaces. It is notable that, during the sliding process, the smooth printing paper gives the smallest current fluctuation of 52%, the sandpaper (#800) with the medium roughness gives an increased fluctuation of 240%, and the highest current fluctuation of 500% is observed for the sandpaper (#120) which has the largest roughness, indicating our skin sensor has the potential application for texture roughness recognition.

2.4. Detection of temperature

Temperature sensing is another vital characteristic of human skin. Thus, in order to mimic the functions of human skin, developing skin sensor device with the capability to feel the temperature is necessary. To demonstrate the ability of our device in detecting temperature,

the sensor was attached on a hotplate and the temperature was well monitored by a thermocouple meter. As shown in **Figure 7**a, the current versus voltage curves were collected from 20 to 130 ^{o}C with a temperature interval of 10 ^{o}C. It is notable that the current decreases with the increase of the temperatures, indicating the capability of our skin sensor for feeling external temperatures. The reduced conductivity of the composite film is because of the expansion of PDMS and thereby the reduced connections between neighboring micro graphite sheets when increasing the temperature. As seen from the current-temperature curve in Figure 7b, the change of the current decreases linearly with the increase of the temperature, and an estimated temperature sensitivity $S_{Temperature}$ = -0.008 $^{o}C^{-1}$ is obtained for our skin sensor, which is comparable with the previously reported temperature sensors.[42-43] The temperature sensitivity $S_{Temperature,}$ is defined as $(\Delta I/I_0)/\Delta T$, where ΔI, I_0, and ΔT are change of current, initial current, and change of temperature, respectively. In another demonstration, a skin sensor was attached on the outside of a beaker to measure the current responses to different temperatures when the beaker was filled with cold water (4 ^{o}C), room-temperature (RT) water (25 ^{o}C), and hot water (80 ^{o}C), respectively. As shown in Figure 7c, almost no obviously current change was observed with filling room-temperature water, whereas notable current increase and decrease were obtained when filling cold and hot water, respectively. Detectable resolution is a vital characteristic of the temperature sensor, and a higher resolution means more accuracy of the sensor device. As depicted in Figure S5 (see in Supporting Information), our skin sensor shows a detectable resolution of 1 ^{o}C in sensing temperature, which is comparable with the recent reported temperature sensors based on the composite films.[42] The above testing results also demonstrate that our skin sensor can well mimic the functionality of the fingertip skin in sensing temperature, indicating its potential application as artificial skin for temperature detection.

3. Conclusion

In conclusion, we present a simple and efficient approach to prepare the porous@microstructured G/PDMS film for multifunctional skin sensors. Due to the unique design, the novel skin sensor has the multiple capabilities to detect pressure, recognize the texture roughness, and sense the temperature. The skin sensor exhibits an ultrahigh sensitivity over a wide linearity range, a low limit of detection, a fast response speed, and a long-term durability in sensing pressure. In addition, the skin sensor shows a high performance in recognition of texture roughness and detection of temperature. The excellent sensing properties of the skin sensors allow the detection of real-time subtle wrist pulses and large motions including bending states of fingers and wrist, and walking states. Moreover, no costly materials or sophisticated equipment are used during the whole fabrication process of the skin sensors. We firmly believe this work could contribute significantly to advance the development of high performance and cost-effective multifunctional skin sensors with promising potential applications in medical diagnosis and artificial intelligence.

4. Experimental Section

Materials: The PDMS base ((Sylgard 184)) and curing agent were bought from Dow Corning Co., Ltd. Graphite sheets were purchased from Beijing Jinglong Tetan Technology Co., Ltd. The sodium chloride powder and ITO/PET substrate (thickness: ITO~100 nm and PET~100 μm) were ordered from Sigma-Aldrich. Commercial available sandpapers with different roughness (Flying Parrot Brand, Korea) were obtained from market.

Fabrication of microstructured PDMS substrate: Firstly, the PDMS base mixed thoroughly with the curing agent at a base to curing agent weight ratio of 5:1 and placed in a gentle vacuum condition at room temperature to remove the air bubbles generated during the agitation process of mixture. The prepolymer was then coated on the sandpaper template (#120) with a blading method followed by covering ITO/PET film on top. After that, the

prepolymer was thermal annealed at 100 ^{o}C for 1 h in a vacuum oven and the one side microstructured PDMS on ITO/PET (denoted as ITO/PET/PDMS) substrate was obtained after removal of the template.

Fabrication of microstrcutured G/PDMS foams: The sandpaper (#120) and NaCl powders were employed as the templates to obtain microstructures on the surface and pores inside of the G/PDMS composite film, respectively. First, after the PDMS base and the curing agent was thoroughly mixed, NaCl powder and graphite sheets were added into the prepolymer, followed by a mechanical agitation for 20 min. Composite inks with different compositions (mass ratio of PDMS, graphite and NaCl = 10:8:X, X=8 or 0) were prepared to fabricate the composite films. Second, after removal of air bubbles generated in the process of mechanical agitation, the composite ink was poured onto the sandpaper template and spread with a doctor blade, followed by covering another piece of sandpaper on top to obtain composite films with double-sided microstructures. In this process, two pieces of glass stripes with a thickness of 1 mm were used to control the thickness of the composite film. Third, the wet composite films were solidified at 100 ^{o}C for 1 h under a gentle vacuum condition. After that, the sandpaper templates were peeled off and the NaCl sacrificial templates were dipped into hot water and dissolved after 2 h under sonication. Finally, porous@microstructured G/PDMS composite film was obtained after drying the samples in a vacuum oven for 2 h. Additionally, for the porous@planar and microstructured only G/PDMS composite films, the fabrication procedures were similar with that of porous@microstructured one, but the sandpaper templates were replaced with the PET substrates for porous@planar one and no NaCl templates were employed for microstructured only one, respectively.

Fabrication of skin sensors: The as prepared composite films were cut into regular size (1 cm × 1 cm) and sandwiched between one ITO/PET substrate and another ITO/PET/PDMS substrate, followed by attaching the copper wires onto the ITO films to complete the sensor fabrication.

Characterization of materials, composite film, and skin sensor: The morphology of graphite sheets, templates, PDMS film, and the composite films were characterized using scanning electron microscopy (SEM, 15 kV, JEOL, JSM-6490). The mechanical test was carried out with a measurement system containing a motorized test stand connected with a force gauge (Mark-10) and electrical signals were collected by a semiconductor parameter analyzer (Agilent 4155C). For the collection of the wrist pulse waveform, the skin sensor was attached to the wrist of a 30-year-old volunteer assisted by medical tape. For the finger bending and wrist bending test, the skin sensors were affixed to the rubber glove using polyimide (PI) tapes. To monitor the moving states of the volunteer, the skin sensor was attached the heel of the volunteer in the whole process of test. For the temperature sensing, the temperature of skin sensor was controlled with a hotplate (IKA) connected with a thermocouple meter.

Supporting Information
Supporting Information is available from the Wiley Online Library or from the author.

Acknowledgements
The authors acknowledge the grant from the Research Grant Council of HKSAR (Grant No. T42-103/16) and the Science and Technology Innovation Commission of Shenzhen (Grant Nos. KQJSCX20170327150812967 and JCYJ20170818143618288)

Received: ((will be filled in by the editorial staff))
Revised: ((will be filled in by the editorial staff))
Published online: ((will be filled in by the editorial staff))

References

[1] D. Chen,Q. Pei. *Chem. Rev.* **2017**, *117*,11239-11268.

[2] D. H. Ho, Q. Sun, S. Y. Kim, J. T. Han, D. H. Kim, J. H. Cho, *Adv. Mater.* **2016**, *28*, 2601-8.

[3] Z. Lou, S. Chen, L. Wang, K. Jiang, G. Shen, *Nano Energy* **2016**, *23*, 7-14.

[4] C. Mu, Y. Song, W. Huang, A. Ran, R. Sun, W. Xie, H. Zhang, *Adv. Funct. Mater.*

2018, *28*, 1707503.

[5] L. Nela, J. Tang, Q. Cao, G. Tulevski, S. J. Han, *Nano Lett.* **2018**, *18*, 2054-2059.

[6] J. Park, M. Kim, Y. Lee, H. Lee, H. Ko, *Sci. Adv.* **2015**, *1*, e1500661.

[7] C. M. Boutry, M. Negre, M. Jorda, O. Vardoulis, A. Chortos, O. Khatib, Z. Bao, *Sci. Robot.* **2018**, *3*, eaau6914.

[8] G. Bermúdez, H. Fuchs, L. Bischoff, J. Fassbender, D. Makarov, *Nat. Electron.* **2018**, *1*, 589-595.

[9] B. C. Tee, C. Wang, R. Allen, Z. Bao, *Nat. Nanotechnol.* **2012**, *7*, 825-32.

[10] Q. Wang, M. Jian, C. Wang, Y. Zhang, *Adv. Funct. Mater.* **2017**, *27*, 1605657.

[11] G. Schwartz, B. Tee, J. Mei, A. Appleton, D. H. Kim,H. Wang, Z. Bao, *Nat. Commun.* **2013**, *4*, 1859.

[12] S. Chen, Y. Song, F. Xu, *ACS Appl. Mater. Interfaces* **2018**, *10*, 34646-34654.

[13] L. Zhang, H. Li, X. Lai, T. Gao, J. Yang, X. Zeng *ACS Appl. Mater. Interfaces* **2018**, *10*, 41784-41792.

[14] S. Gong, W. Schwalb, Y. Wang, Y. Chen, Y. Tang, J. Si, B. Shirinzadeh, W. Cheng, *Nat. Commun.* **2014**, *5*, 3132.

[15] X. Han, X. Chen, X. Tang, Y.-L. Chen, J.-H. Liu, Q.-D. Shen, *Adv. Funct. Mater.* **2016**, *26*, 3640-3648.

[16] N. Luo, W. Dai, C. Li, Z. Zhou, L. Lu, C. C. Y. Poon, S.-C. Chen, Y. Zhang, N. Zhao, *Adv. Funct. Mater.* **2016**, *26*, 1178-1187.

[17] K.-Y. Shin, J. S. Lee, J. Jang, *Nano Energy* **2016**, *22*, 95-104.

[18] Y. Song, H. Chen, Z. Su, X. Chen, L. Miao, J. Zhang, X. Cheng, H. Zhang, *Small* **2017**, *13*.

[19] T. Q. Trung, N. E. Lee, *Adv. Mater.* **2016**, *28*, 4338-72.

[20] X. Wang, Y. Gu, Z. Xiong, Z. Cui, T. Zhang, *Adv. Mater.* **2014**, *26*, 1336-42.

[21] Y. Wang, L. Wang, T. Yang, X. Li, X. Zang, M. Zhu, K. Wang, D. Wu, H. Zhu, *Adv.*

Funct. Mater. **2014**, *24*, 4666-4670.

[22] Y. Ai, T. Hsu, D. Wu, L. Lee, J. Chen, Y.- Chen, S.Wu, C. Wu, Z. M. Wang, Y. Chueh *J. Mater. Chem. C* **2018**, *6*, 5514-5520.

[23] Y. Zang, F. Zhang, C. A. Di, D. Zhu, *Mater. Horiz.* **2015**, *2*, 140-156.

[24] Y. Zang, F. Zhang, D. Huang, X. Gao, C. A. Di, D. Zhu, *Nat. Commun.* **2015**, *6*, 6269.

[25] A. Gerratt, H. Michaud, S. Lacour, *Adv. Funct. Mater.* **2015**, *25*, 2287-2295.

[26] J. Byun, Y. Lee, J. Yoon, B. Lee, E. Oh, S. Chung, T. Lee, K. Cho, J. Kim, Y. Hong, *Sci. Robot.* **2018**, *3*, eaas9020.

[27] Z. Lei, Q. Wang, S. Sun, W. Zhu, P. Wu, *Adv. Mater.* **2017**, *29*.

[28] K. Parida, V. Bhavanasi, V. Kumar, R. Bendi, P. S. Lee, *Nano Res.* **2017**, *10*, 3557-3570.

[29] B. Zhu, Z. Niu, H. Wang, W. R. Leow, H. Wang, Y. Li, L. Zheng, J. Wei, F. Huo, X. Chen, *Small* **2014**, *10*, 3625-31.

[30] S. Chen, Y. Song, D. Ding, Z. Ling, F. Xu, *Adv. Funct. Mater.* **2018**, *28*, 1802547.

[31] J.-H. Lee, *Sens. Actuators B* **2009**, *140*, 319-336.

[32] Y. Cao, T. Li, Y. Gu, H. Luo, S. Wang, T. Zhang, *Small* **2018**, *14*, e1703902.

[33] H. Chang, S. Kim, S. Jin, S. W. Lee, G. T. Yang, K. Y. Lee, H. Yi, *ACS Appl. Mater. Interfaces* **2018**, *10*, 1067-1076.

[34] K. Y. Lee, H.-J. Yoon, T. Jiang, X. Wen, W. Seung, S.-W. Kim, Z. L. Wang, *Adv. Energy Mater.* **2016**, *6*, 1502566.

[35] Q. Shao, Z. Niu, M. Hirtz, L. Jiang, Y. Liu, Z. Wang, X. Chen, *Small* **2014**, *10*, 1466-1472.

[36] B. Su, S. Gong, Z. Ma, L. W. Yap, W. Cheng, *Small* **2015**, *11*, 1886-91.

[37] K. Xia, C. Wang, M. Jian, Q. Wang, Y. Zhang, *Nano Res.* **2017**, *11*, 1124-1134.

[38] M. Ha, S. Lim, J. Park, D.-S. Um, Y. Lee, H. Ko, *Adv. Funct. Mater.* **2015**, *25*, 2841-2849.

[39] P. Nie, R. Wang, X. Xu, Y. Cheng, X. Wang, L. Shi, J. Sun, *ACS Appl. Mater. Interfaces* **2017**, *9*, 14911-14919.

[40] J. H. Oh, S. Y. Hong, H. Park, S. W. Jin, Y. R. Jeong, S. Y. Oh, J. Yun, H. Lee, J. W. Kim, J. S. Ha, *ACS Appl. Mater. Interfaces* **2018**, *10*, 7263-7270.

[41] Y. Wei, S. Chen, Y. Lin, Z. Yang, L. Liu, *J. Mater. Chem. C* **2015**, *3*, 9594-9602.

[42] Z. Lou, S. Chen, L. Wang, R. Shi, L. Li, K. Jiang, D. Chen, G. Shen, *Nano Energy* **2017**, *38*, 28-35.

[43] T. Q. Trung, S. Ramasundaram, B. U. Hwang, N. E. Lee, *Adv. Mater.* **2016**, *28*, 502-9.

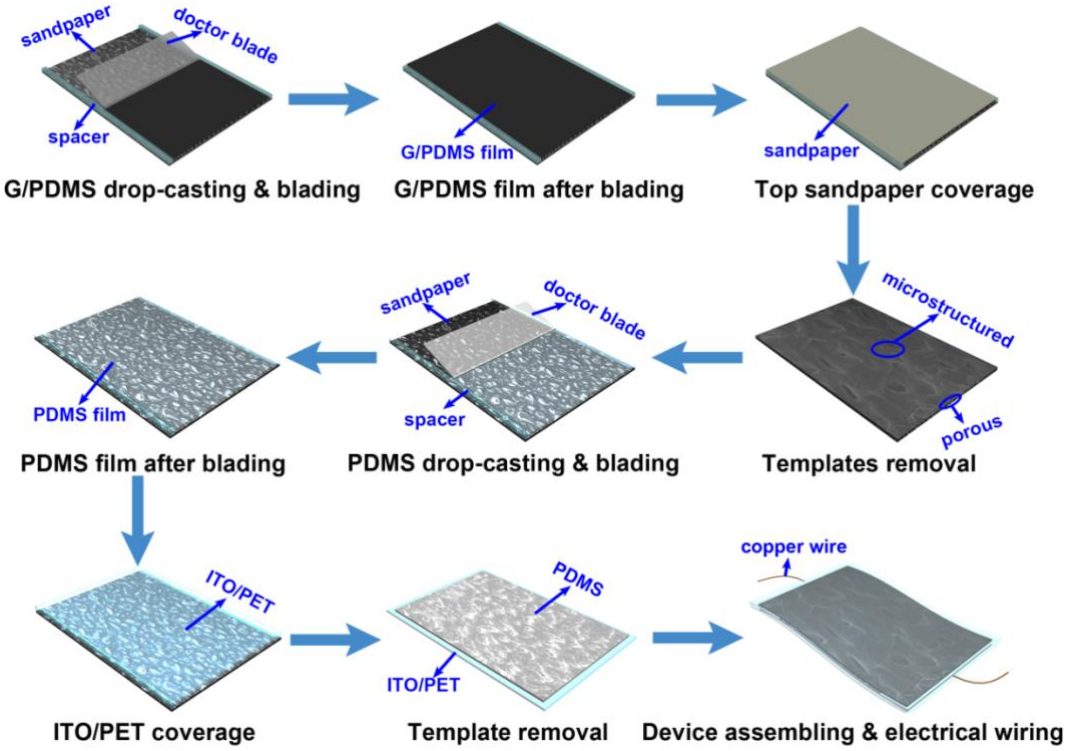

Figure 1. Schematic of the whole fabrication process for the multifunctional skin sensor with G/PDMS composite film.

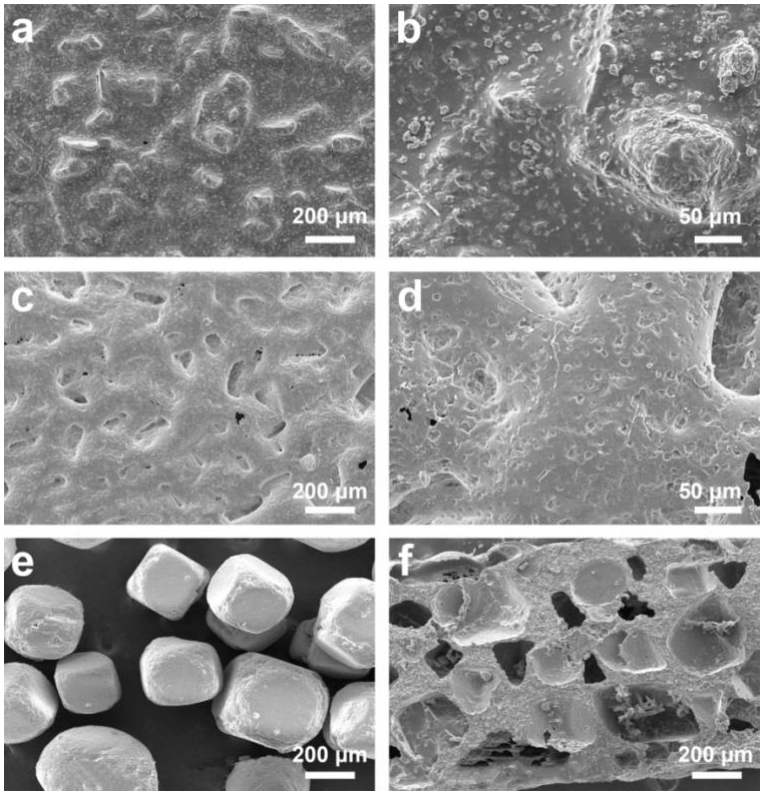

Figure 2. a) and b) SEM images of the sandpaper template in different magnifications. c) and d) SEM images of the G/PDMS film in different magnifications. e) SEM image of NaCl template. f) SEM image of cross-sectional view of the G/PDMS composite film.

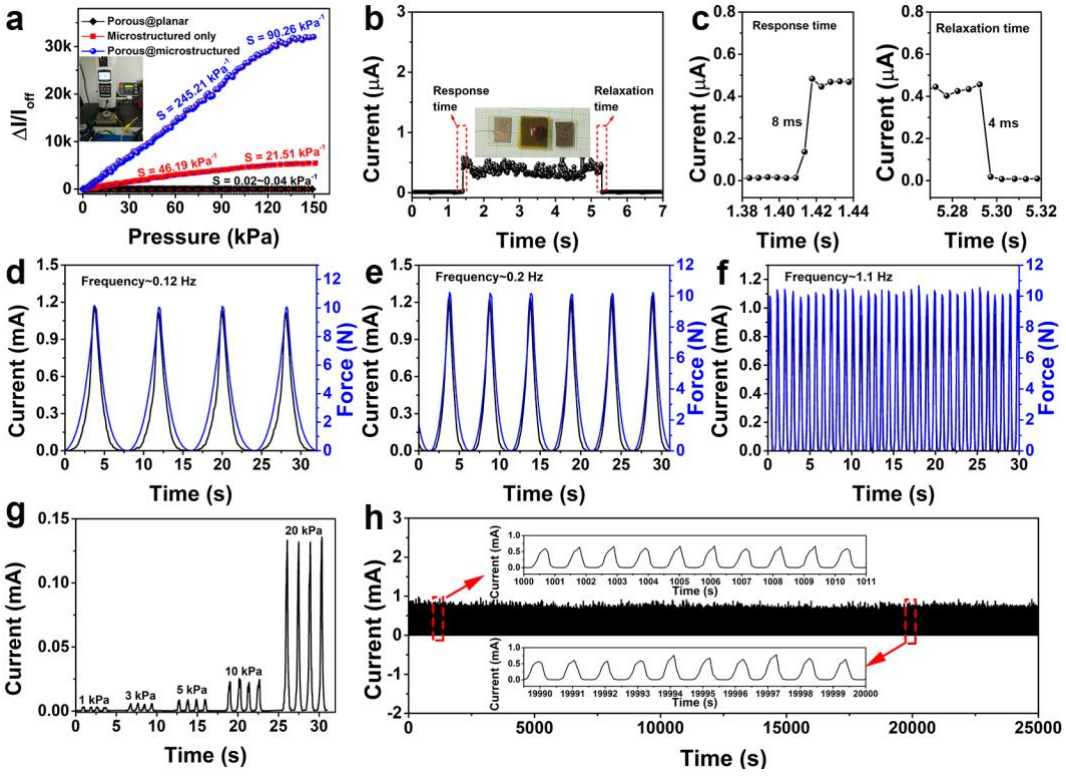

Figure 3. Mechanical property test of the skin sensor. a) Current responses of the skin sensors based on three different G/PDMS composite films to continous pressure from 0 to 150 kPa. Inset is the photograph of the test stand with force gauge. b) Current responses to loading/unloading a red bean (~50 mg) on the skin sensor. Inset is the photograph of a red bean on the skin sensor. c) Response time and relaxation time of the skin sensor estimated from (b). d-f) Cyclic current responsse to 100 kPa at different frequencies, 0.12, 0.20, and 1.10 Hz, respectively. g) Cyclic current responses to diverse pressures. h) Long-term durability test (25 000s) of the skin sensor at a pressure of 100 kPa. Inset: magnified view of 10 cycles for the early (1000 s) and end (20 000s) stages, respectively.

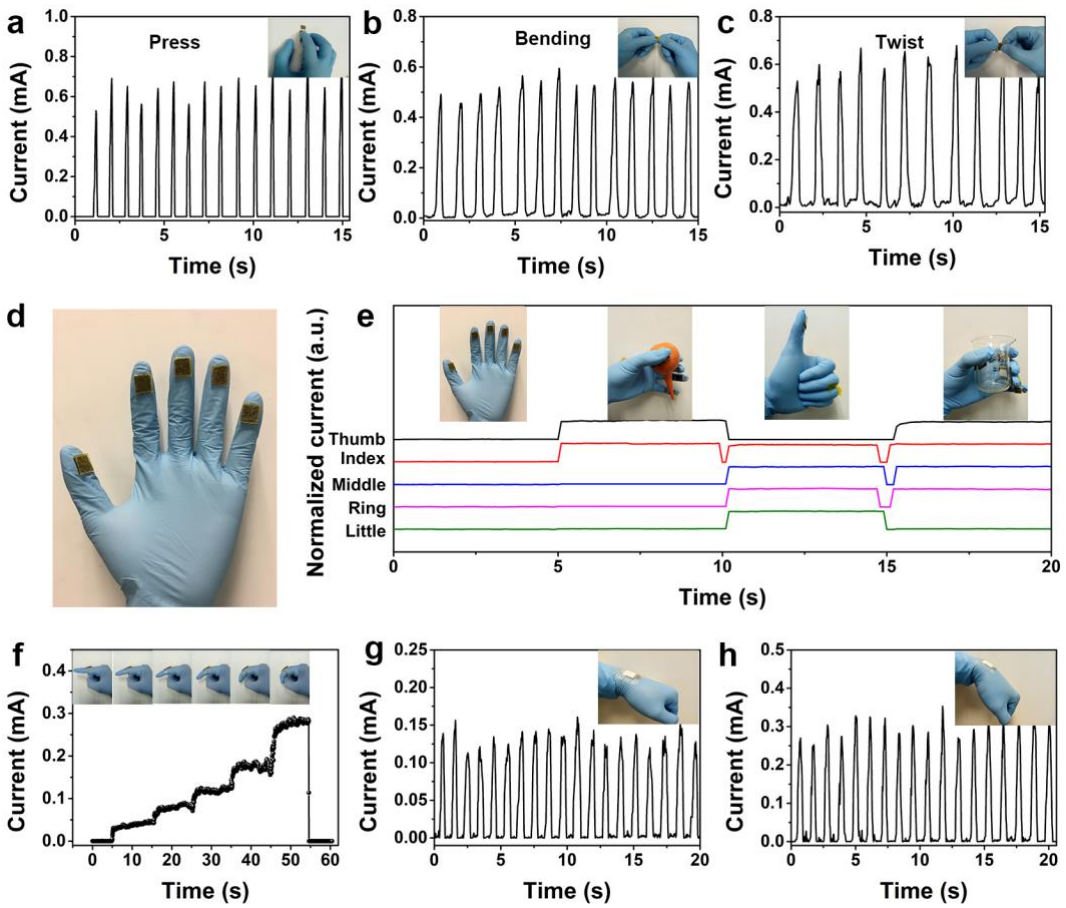

Figure 4. a-c) Current responses to press, bending and twist forces, respectively. d) Photograph of five skin sensors attached on the fingertips of a rubber glove. e) Current responses to various hand motions. f) Real-time current signals in response to finger gesture with different bending angles. g,h) Real-time cyclic test of wrist bending with bending angles of 30 and 60, respectively.

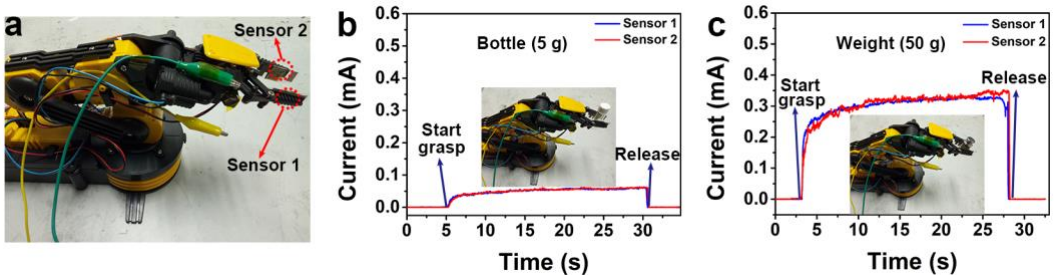

Figure 5. a) Photograph of two skin sensors attached on a robotic arm. Current responses of the skin sensors to the applied pressure in the process of grasping and releasing b) a bottle~5 g and c) a weight~50 g.

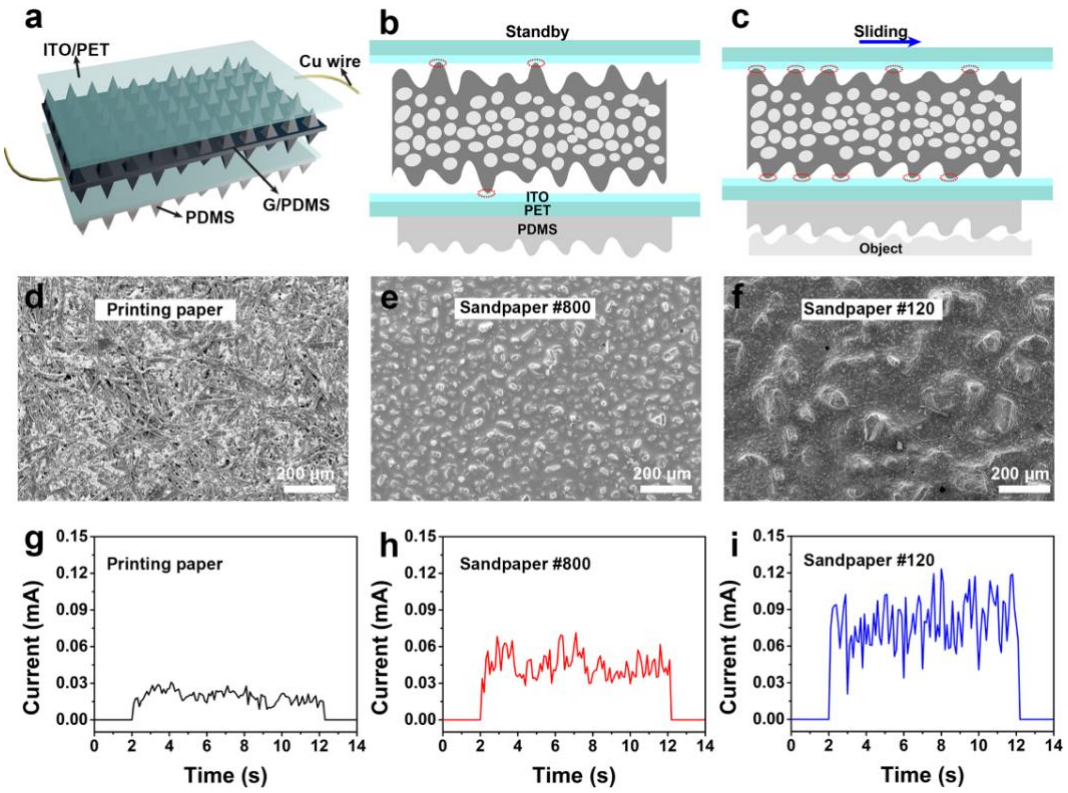

Figure 6. a-c) Schematic illustration of the skin sensor for texture roughness recognization, in which, (a) is the schematic diagram of the skin sensor, (b) and (c) showing the mechanism of the skin sensor in recognizing texture roughness. d-f) SEM images of the surface morphology of the test objects (printing paper, sandpaper #800, and sandpaper #120). g-i) Current signals in response to various texture roughness.

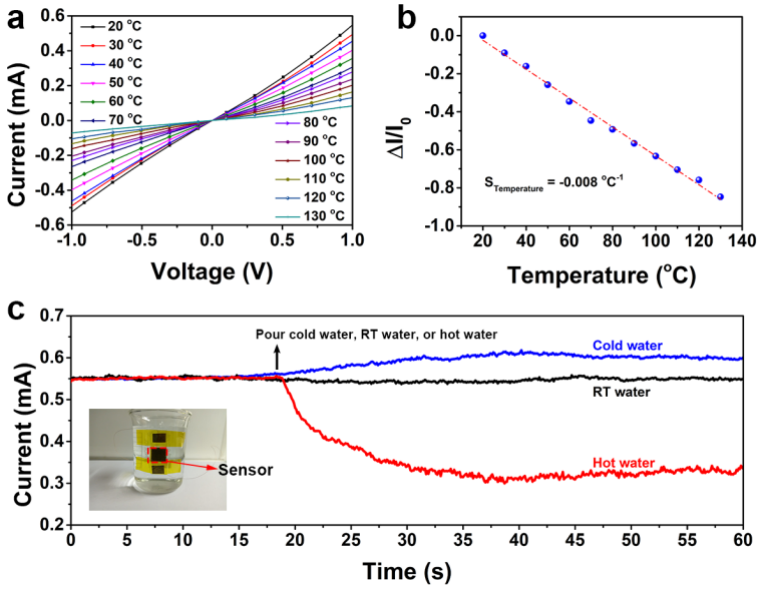

Figure 7. Characterization of the skin sensor in sensing temperature. a) *I-V* curves under different temperatures. b) Relative current change *vs*. temperature. c) Current responses of the skin sensor to water at 4 ^{o}C, 25 ^{o}C and 80 ^{o}C, respectively. The inset shows a skin sensor affixed onto a beaker.

Fingertip skin inspired skin sensors based on hierarchically structured conductive graphite/polydimethylsiloxane (G/PDMS) foams show a high sensitivity in wide pressure range. Furthermore, except sensing pressure, the skin sensor can distinguish the texture roughness and temperature as well. The skin sensor has demonstrated the applications in monitoring physiological signals, distinguishing papers with different texture roughness, and indicating environmental temperatures.

Keyword: skin sensor, hierarchical structure, multifunctional sensing, healthcare monitoring, temperature sensing

Qi-Jun Sun, Xin-Hua Zhao, Ye Zhou, Chi-Chung Yeung, Wei Wu, Shishir Venkatesh, Zong-Xiang Xu*, Jonathan J. Wylie, Wen-Jung Li, and Vellaisamy A. L. Roy*

Fingertip Skin-Inspired Highly Sensitive and Multifunctional Sensor with Hierarchically Structured Conductive Graphite/Polydimethylsiloxane Foams

Table of Contents

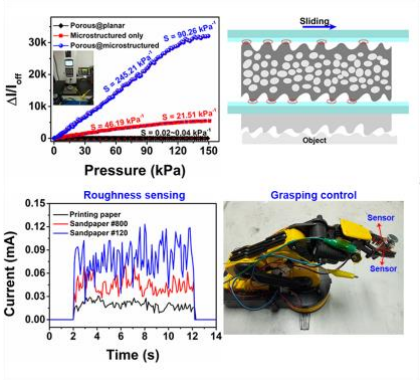

Supporting Information

Fingertip Skin-Inspired Highly Sensitive and Multifunctional Sensor with Hierarchically Structured Conductive Graphite/Polydimethylsiloxane Foams

Qi-Jun Sun, Xin-Hua Zhao, Ye Zhou, Chi-Chung Yeung, Wei Wu, Shishir Venkatesh, Zong-Xiang Xu, Jonathan J. Wylie, Wen-Jung Li, and Vellaisamy A. L. Roy**

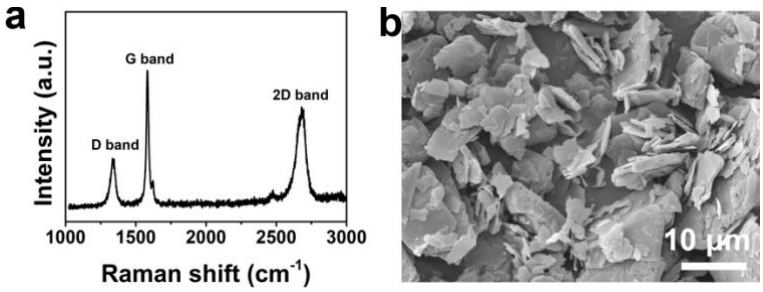

Figure S1. a) Raman spectra and b) SEM image of graphite sheets.

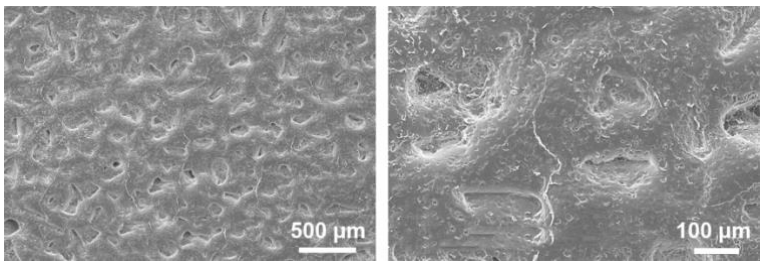

Figure S2. SEM images of surface morphology of microstructured PDMS film displayed in different magnifications.

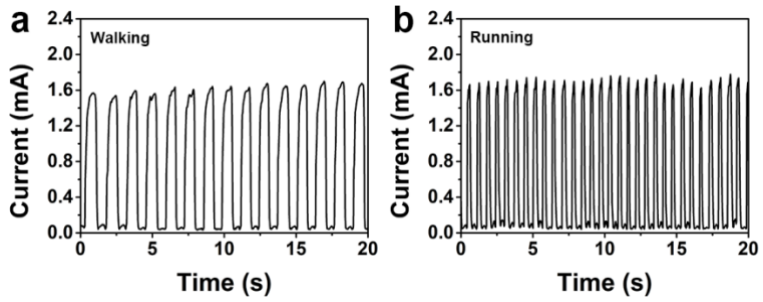

Figure S3. Current responses of the skin sensor to a) walking and b) running.

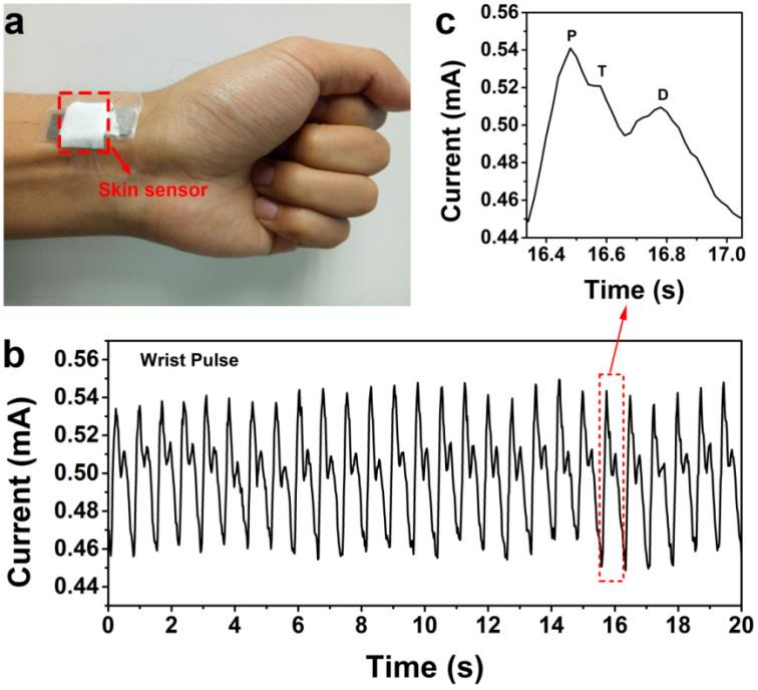

Figure S4. a) The skin sensor attached to the artery of human wrist. b) Wrist pulses collected in real time of a 29-year-old volunteer. c) Enlarged view of a wrist waveform picked from (b), showing three characteristic peaks, P peak, T peak, and D peak.

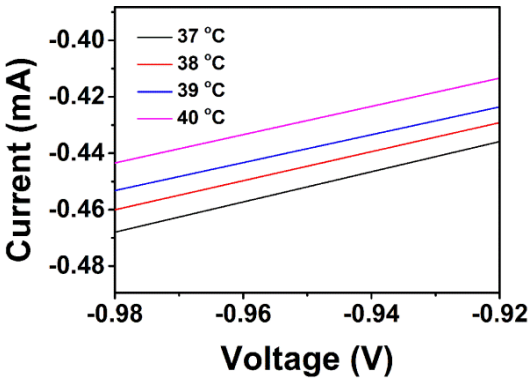

Figure S5. Current-voltage curves of the skin sensor measured at different temperatures. The skin sensor shows a temperature detection resolution < 1 $_{o}$C.

Table S1. Comparasion of the performance of piezoresistive pressure sensors

No.	Sensor type	Response time (ms)	Relaxation time (ms)	LOD (Pa)	Sensing range (kPa)	Sensitivity (kPa^{-1})	References
1	*CNT/Cotton*	18	24	2	20	14.4	1
2	*Au NWs/Tissue paper*	17	N/A	13	5	1.1	2
3	*SWNTs/PDMS*	10	N/A	0.6	1.2	1.8	3
4	*rGO/PDMS with pyramid microstructures*	0.2	N/A	1.5	0.1	5.5	4
5	*MXene/rGO*	245	212	10	3.5	22.5	5

6	*Carbonized melamine foams*	N/A	N/A	3	2	100.3	6
7	*Aligned carbon nanotubes/Graphene /PDMS*	N/A	N/A	0.6	0.3	19.8	7
8	*Wrinkled graphene/Polyvinyl alcohol nanowires*	N/A	N/A	2.2	14	28.3	8
9	*Polypyrrole hollow sphere*	47	N/A	0.8	0.03	133.1	9
10	*Microstructured@porous G/PDMS*	8	4	5	120	245.2	This work

Reference

[1] M. Liu, X. Pu, C. Jiang, T. Liu, X. Huang, L. Chen, C. Du, J. Sun, W. Hu, Z. L. Wang, *Adv. Mater.* **2017**, *29*.

[2] S. Gong, W. Schwalb, Y. Wang, Y. Chen, Y. Tang, J. Si, B. Shirinzadeh, W. Cheng, *Nat. Commun.* **2014**, *5*, 3132.

[3] X. Wang, Y. Gu, Z. Xiong, Z. Cui, T. Zhang, *Adv. Mater.* **2014**, *26*, 1336-42.

[4] B. Zhu, Z. Niu, H. Wang, W. R. Leow, H. Wang, Y. Li, L. Zheng, J. Wei, F. Huo, X. Chen, *Small* **2014**, *10*, 3625-31.

[5] Y. Ma, Y. Yue, H. Zhang, F. Cheng, W. Zhao, J. Rao, S. Luo, J. Wang, X. Jiang, Z. Liu, N. Liu, Y. Gao, *ACS Nano* **2018**, *12*, 3209-3216.

[6] W. Liu, N. Liu, Y. Yue, J. Rao, C. Luo, H. Zhang, C. Yang, J. Su, Z. Liu, Y. Gao, *J. Mater.Chem.C* **2018**, *6*, 1451-1458.

[7] M. Jian, K. Xia, Q. Wang, Z. Yin, H. Wang, C. Wang, H. Xie, M. Zhang, Y. Zhang, *Adv. Funct. Mater.***2017**, *27*, 1606066.

[8] W. Liu, N. Liu, Y. Yue, J. Rao, F. Cheng, J. Su, Z. Liu, Y. Gao, *Small* **2018**, *14*, e1704149.

[9] L. Pan, A. Chortos, G. Yu, Y. Wang, S. Isaacson, R. Allen, Y. Shi, R. Dauskardt, Z. Bao, *Nat. Commun.* **2014**, *5*, 3002.